PAPER • **OPEN ACCESS**

Influence of direct current (DC) on mild steel coating stainless steel rods via TIG welding: A model for the rehabilitation of steel components

To cite this article: M.N. Muigai *et al* 2021 *IOP Conf. Ser.: Mater. Sci. Eng.* **1107** 012039

Influence of direct current (DC) on mild steel coating stainless steel rods via TIG welding: A model for the rehabilitation of steel components

M.N. Muigai[1], F.M. Mwema[1,2,*], E.T. Akinlabi[2] and J.O. Obiko

[1]Department of Mechanical Engineering, Dedan Kimathi University of Technology, 10100.Nyeri, Kenya.
[2] Department of Mechanical Engineering Science, University of Johannesburg, South Africa.
[3]Department of Mining, Material and Petroleum Engineering, Jomo Kenyatta University of Agriculture & Technology, Nairobi Kenya.
Corresponding Author; fredrick.mwema@dkut.ac.ke

Abstract-
In this paper, the influence of varying DC current on microstructures of mild steel substrates coated with stainless steel using TIG welding technique was investigated. To achieve the desired results, mild steel substrates of sizes 40 mm × 10 mm × 1.5 mm were used. The mild steel substrates were ground using Silicon Carbide (SiC) papers to achieve smooth surfaces and to remove oxides that might be present on their surfaces. Then the substrates were coated using stainless-steel rods on TIG 2200i AC/DC machine as a welding power source. The process was undertaken under six varying currents of 40 A, 50 A, 55 A, 60 A, 65 A and 70 A. For purpose of characterization, microstructures of the coated samples were studied using optical microscopy and quantitative image analyses. The depth of penetration of the melt pool below the substrates and the coating thickness were measured for all the samples. Based on the optical microscopy, four zones were identified on the TIG coated samples; the heat-affected zone (HAZ), fusion, coating and a skirt (the region that formed between the substrates and the coatings). Minute porosities were also observed in the coated samples. It was observed that the maximum coating thickness was 5.345 mm and the highest average coating thickness was 3.522 mm, which both occurred at 40 A. The maximum length of penetration was 3.864 mm and was observed when 60 A DC was used. Similarly, the highest average depth of penetration was 2.422 mm and occurred at 65 A. The results of this study showed that for direct current, as the current increased from 40 A to 50 A, the porosities in the coated samples increased. However, at 55 A, the number of porosities decreased, but continued to increase from 60 A to 65 A, but the porosities decreased again at 70 A.

Keywords: Coating, current, microstructure, mild steel, stainless steel, TIG welding

1. Introduction

Welding is the widely utilized thermal technique for joining metallic parts. There are various welding techniques, and one of them is the tungsten inert gas (TIG) welding. The technique (TIG) welding, which is also known as Gas tungsten arc welding (GTAW) uses a consumable electrode which melts between a metallic workpiece and a non-consumable tungsten electrode [1]. This Technology is preferred over the other arc-based welding technologies since it operates within shielded conditions and allows the user to control various parameters of the

process [2]–[4]. It is worth noting that there is inexhaustible literature on TIG welding of different materials with an emphasis on the optimization of the welding process parameters [5]–[9].

Apart from joining metals together, welding is used in rehabilitating steel structures that have severely experienced natural disasters and as a result of wear and corrosion failures which occur on such structures during their operation in different conditions [10]. Therefore, to prevent them from collapsing, rehabilitation is needed [11], [12]. Repair welding usually involves rehabilitating steels that are difficult to weld including quenched, high carbon, wear-resistant, tempered, tool-making as well as spring steels. Applications of repair welding include in the rehabilitation of damaged shafts, machine components and gears. Tanasković et al., 2017, studied the use of welding methods to repair eight gear shafts that had been damaged as a result of exploitation conditions which caused the teeth of the gear to wear laterally. In this case, manual arc welding was used, and it proved to be successful [11]. In another study, a worn-out low carbon steel shaft was repaired via discontinuous arc welding as a model for local rehabilitation of machine components [13]. It was shown that this approach increased the hardness and wear properties of the shaft without interfering with its tensile strength.

Other related studies include [14]–[16], and it can be observed that there are very few research groups around the world researching on welding as a repair alternative for components despite being utilized in many light industries in developing countries. To contribute to this under-researched concept, the authors in this paper have investigated the effect of TIG DC current on the evolving microstructure of mild steel substrates coated with stainless steel rods.

2. Experimental Methods

In this study, mild steel substrates of sizes 40 mm × 10 mm × 1.5 mm were ground using SiC papers to fine surfaces and to clean off surface oxides. After which the mild steel substrates were cleaned with acetone and dried. Then, the substrates were coated with stainless-steel rods using TIG 2200i AC/DC machine as a welding power source. The process was undertaken using a direct current (DC) at different currents of the TIG machine. The currents used were 40 A, 50 A, 55 A, 60 A, 65 A and 70 A. The welding was undertaken manually by an experienced welder in the manufacturing centre for all the samples. Figure 1 shows the pictorial representation of the prepared samples.

Figure 1:Stainless steel coated mild steel samples at different DC currents

Samples with a cross-section of 5 mm by 3 mm were cut from the coated samples for metallographic analysis. The cut samples were mounted along the cross-section by hot mounting using Polyfast resin. After mounting, the samples were ground and polished using standard metallographic procedures. The ground and polished samples were etched with Villella's reagent for microstructure investigation using a Leica DM 6000M optical microscope.

On the optical microscope, the imaging was undertaken along the coating-substrate cross-section to undertake the various zones and interactions between the two materials. The optical images obtained were analysed using ImageJ software to determine the depth of penetration of the melt pool as well as the coating thickness obtained for each experiment. For each quantification, ten measurements were taken, and the average was reported for statistical accuracy of the results.

3. Results and discussion

Metal coating using TIG welding technique was achieved for mild steel samples. The coating material (stainless steel) and the substrate were melted to form a melt pool. The melt pool penetrated through the substrate and as a result a metallurgical bond was formed between the coating material and the substrate. The results obtained for this study were analysed in terms of depth of penetration, thickness of the coating and porosity as described in the respective sections.

3.1 Depth of Penetration

The depth of penetration of the melt pool into the mild steel samples was analysed. Ten measurement on the depth of penetration were taken on each coated sample, and then an average depth was determined using ImageJ software. Figure 2 illustrates the depth of penetration, thickness of the coating and the measurement procedure.

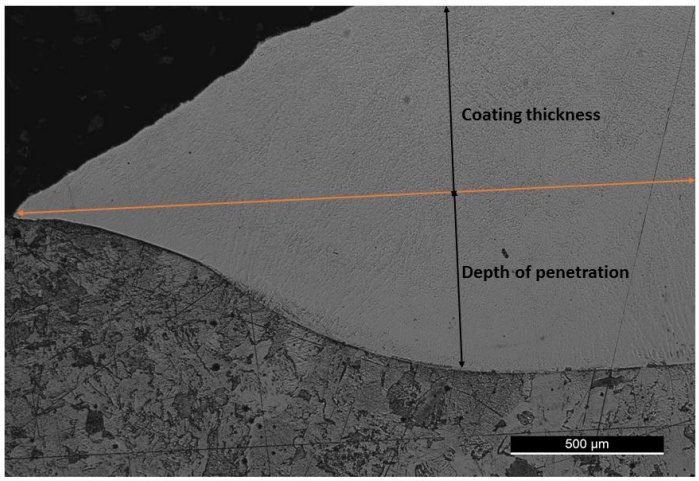

Figure 2: Illustrating the methodology for measurement of depth of penetration and coating thickness. The image shown was obtained at a DC current of 65A

The measurements of the depth of penetration taken are recorded in Table 1 while their corresponding average values are presented in Table 2.

Table 1: Depth of penetration of the melt pool

Current	Length (mm)									
40 A	0.347	0.480	0.653	0.840	1.04	1.134	1.166	1.043	0.965	0.347
50 A	0.254	0.480	0.928	1.490	2.60	3.560	3.478	3.520	3.494	3.481
55 A	0.280	0.400	0.733	1.107	1.560	1.935	2.162	2.274	2.269	2.163
60 A	0.308	0.750	1.187	1.533	2.163	2.514	4.407	3.82	3.854	3.801
65 A	0.747	1.520	1.987	2.188	2.415	2.528	2.655	3.099	3.534	3.641
70 A	0.24	0.494	0.961	1.507	1.720	1.760	1.787	1.722	2.054	2.227

Table 2: Average depth of penetration

Direct current	40 A	50 A	55 A	60 A	55 A	70 A
Mean Length (mm)	0.843	2.328	1.492	2.334	2.422	1.447
Standard deviation	0.280	1.391	0.792	1.352	0.882	0.527
Minimum length (mm)	0.347	0.254	0.280	0.308	0.747	0.240
Maximum length (mm)	1.166	3.560	2.274	3.854	3.641	2.054

The data (Tables 1 and 2) on the mean and maximum depth of penetration were plotted as functions of the DC TIG current as shown in Figure 3.

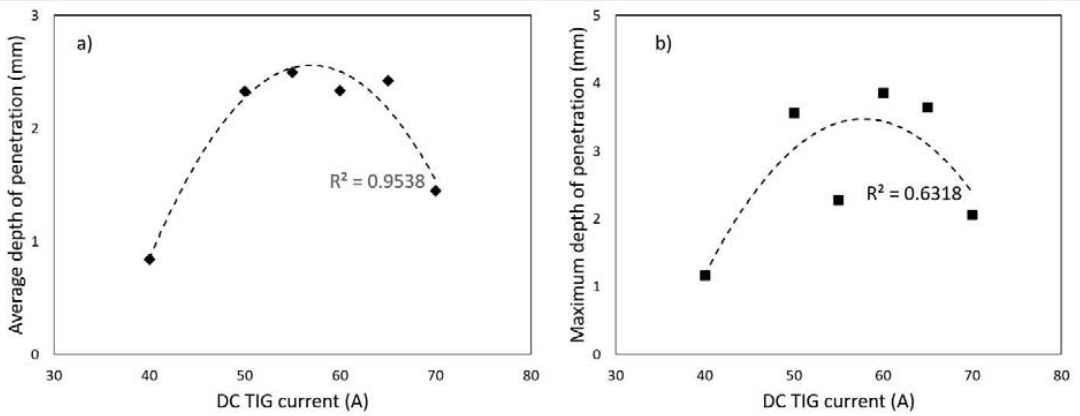

Figure 3: Graphs of (a) mean depth of penetration and (b) maximum depth of penetration against DC TIG current. The dotted lines indicate the quadratic approximation of the trends of the data points. The R^2 values indicate the regression coefficients

As shown, it was observed that the mean depth of penetration when direct current was used, was lowest at 40 A and highest at 65 A. Generally, there was no linear relationship between the depth of penetration and DC current of the welding process. A quadratic polynomial however (with a regression coefficient of 0.95 and 0.63 respectively) was shown to be a good approximation of the trend. The relationship exhibited a 'hook-like' shape, which generally

means that the depth of penetration increases to a maximum point at some current and then falls to a minimum value as the current increases. The mean depth of penetration of the melt pool into the mild steel sample increased as the current increased from 40 A to 50 A, however at 55 A, the depth of penetration decreased. At 60 A direct current, the depth of penetration of the melt pool started to increase again with 65 A having the highest average depth of penetration. However, at 70 A the average depth of penetration decreased as shown in Figure 3(a). The maximum length of penetration was 3.864 mm and was observed when 60 A direct current was used as shown in Figure 3(b). Similarly, the highest average depth of penetration was 2.422 mm and occurred at 65 A as shown in Figure 3(a). As the coating current increased, large amount of heat energy was introduced into a coating zone, which made a lot of melt pool to penetrate the substrate, therefore large depths of penetration were observed [17].

3.2 Coating thickness

Similarly, the thickness of the coatings achieved was measured using ImageJ software. The results obtained were recorded in Tables 3 and 4 and plotted graphs in Figure 4. As shown, generally, there was no linearity between the coating thickness and the welding current. A polynomial approximation of order 3 was fitted in the data with a closeness of fit value of about R^2=0.7 and it can be deduced that thickness coating generally decreased with the welding current up to a minimum saturation value of thickness. According to Figure 4(b), it was observed that the highest average coating thickness was 3.522 mm and it occurred when 40 A direct current was used. The average coating thickness reduced from 3.52 mm (at 40 A) to 2.505 mm at 50 A. At currents between 50 A and 55 A, the coating thickness increased slightly. However, between 55 A and 60 A, the thickness decreased rapidly beyond which coating thickness decreased up to 70 A. From Figure 4(a), the maximum coating thickness (5.345 mm) was observed to occur when 40 A direct current was used. The average saturation thickness was shown to be about 1.755 mm and occurred between 65 and 70 amperes. At high current, huge amount of heat produced resulted to a lot of melt pool penetrating the substrate, as a result, little melt pool was left to form the coating required, because most of it penetrated into the substate.

Table 3: Measured coating thickness at various DC TIG currents

Current	Length (mm)									
40 A	0.700	1.420	2.260	3.12	3.601	4.042	4.545	4.861	5.325	5.345
50 A	0.520	1.240	1.861	2.560	3.020	3.223	3.160	3.201	3.161	3.100
55 A	1.204	2.183	2.821	3.283	3.281	3.300	3.300	3.34	3.280	3.283
60 A	0.261	0.520	0.880	1.820	2.484	2.962	3.320	3.640	3.80	4.020
65 A	0.180	0.600	1.161	1.762	2.143	2.301	2.320	2.380	2.203	2.500
70 A	0.660	1.201	1.521	2.083	2.320	2.840	3.141	3.300	3.400	3.501

Table 4: Average values of the measured coating thickness at various direct currents

Direct current	40 A	50 A	55 A	60 A	55 A	70 A
Mean Length (mm)	3.522	2.505	2.928	2.371	1.755	2.397
Standard deviation	1.627	0.968	0.706	1.416	0.822	1.006
Minimum length (mm)	0.700	0.520	1.204	0.261	0.180	0.66
Maximum length (mm)	5.345	3.223	3.340	4.020	2.500	3.501

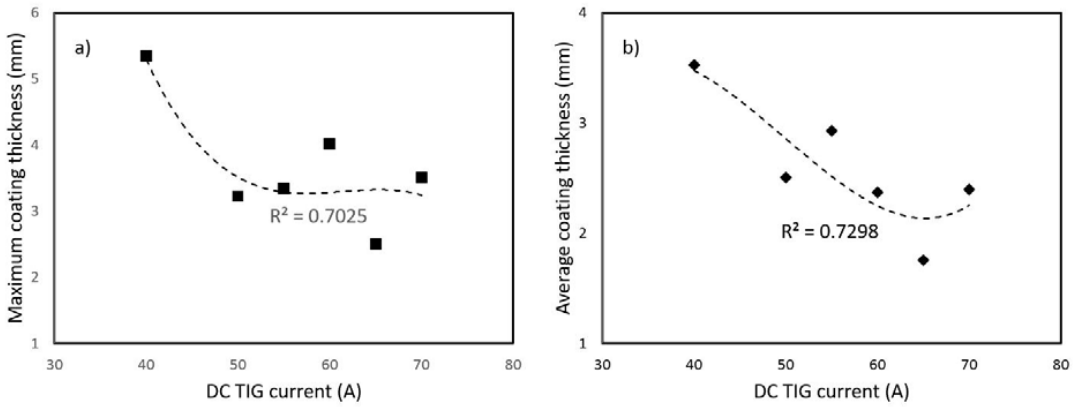

Figure 4: Graphs of maximum coating thickness and average coating thickness against DC TIG current. The dotted lines represent an approximation polynomial of order 3 of the data. The R^2 values indicate the regression coefficients

3.3 Porosity

Based on the optical imaging of the coated samples, four zones were identified along the cross-sections namely, the substrate, fusion, coating and a skirt (region that formed between the substrates and the coatings). It was observed that for all the samples, porosity was present in the coating layer. Figure 5 shows porosity in samples prepared at direct currents of 40 A and 50 A.

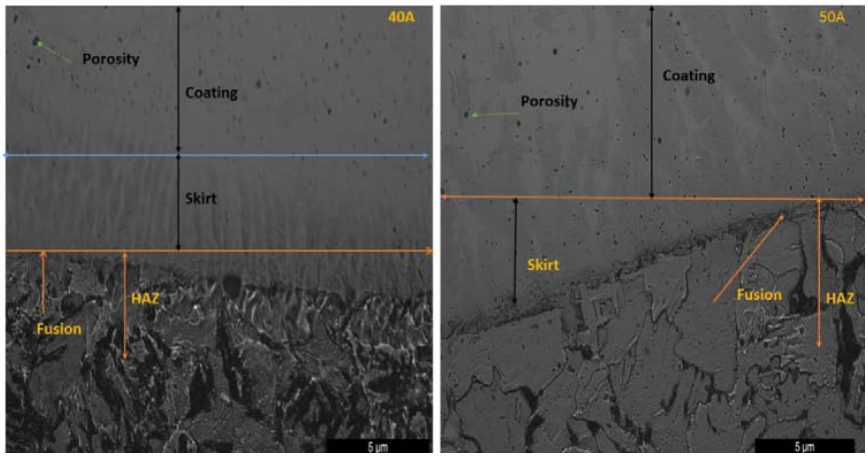

Figure 5: Porosity in mild steel samples coated with stainless steel at 40 A and 50 A TIG direct currents. The coating, fusion, HAZ and skirt regions are identified as well

As shown, the porosities on samples prepared at 40 A were circular in morphology and with varying sizes. The porosity features were distributed evenly within the coating region with very few porous structures observed at the skirt region, fusion and heat affected zone. On the 50 A samples, the number of porous structures appeared visually to have increased as compared to those in the 40 A samples. The porosities were circular in shape and were evenly

distributed in the coating region, heat affected zone, fusion region as well as in the skirt region. Similarly, the size of the porous structures varied across the microstructure.

Figure 6 shows the porosity in samples prepared at 55 A and 60 A TIG direct current. At 55 A, the number of porous features appeared visually fewer than those observed in the sample prepared at 50 A DC current. There were very few porosity features seen in the skirt, heat affected zone and the coating-substrate fusion. These features exhibited circular shape and almost of the same size across the microstructure. At 60 A, the porosity features increased in number as compared to those at 55 A. Some of these porosities were circular while others were elongated. At the heat affected zone and the skirt region, the porosities appear to have occurred close to each other when compared to the distribution of the porosities at the fusion and coating regions.

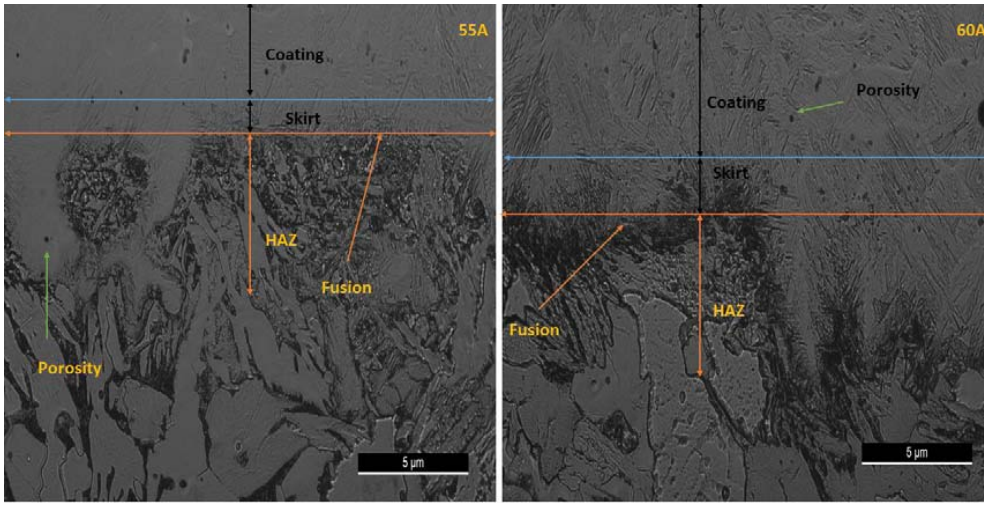

Figure 6: Porosity in mild steel samples coated with stainless steel at 55 A and 60 A TIG direct currents.

Figure 7 shows the porosity features in samples prepared at 65 A and 70 A TIG direct currents. As shown, samples prepared at 65 A direct current exhibited more porosities than those observed in the 60 A samples. The reason for this behaviour was that as the coating current increased, heat energy introduced to the melt pool increased. As a result, a lot of heat lead to more gas bubbles being trapped within the melt pool, which caused more porosities. The size of the porosities differed across the different regions with those on the coating region being larger than those at the HAZ. The reason for this observation was because at the coating region, there was a lot of heat as compared to other regions and as a result, a lot of gases bubbles such as hydrogen and oxygen were trapped within the melt pool and when the melt pool solidified, large porosities were formed [18]. In this case, the fusion region as well as the skirt region had few porosities, with the coating region having the highest distribution of porosities and they were mostly circular in shape. At 70 A, the number of porous structures was seen to reduce as compared to those in the sample prepared at 65 A TIG direct current. The structures in this case were spherical with very small distribution at the heat affected zone,

interface region and the skirt region. The distribution of the porosities in the coating region was higher than in other regions of the coated sample when 65 A was used.

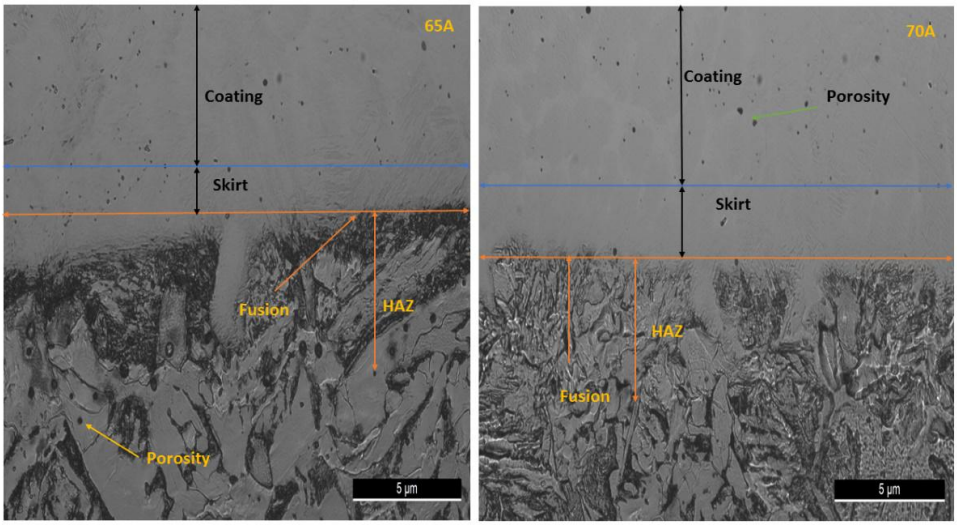

Figure 7: Porosity in mild steel samples coated with stainless steel at 65 A and 70 A TIG direct currents

4. Conclusions

The influence of TIG welding DC current, on coating of mild steel samples using stainless steels rods was studied and reported in this article. The variation of dimensions of the coatings in terms of depth of penetration of the melt pool and coating thickness as well as the presence of porosities has been reported. From this study it can be concluded that the microscopy images of the coated samples revealed four significant zones, namely, the coating, skirt, heat affected zone and the fusion regions. The results of this study showed that as the DC current increased from 40 A to 50 A, the quantity (visually) of porosity features in the coated samples increased. However, at 55 A, the number of porous structures decreased, but continued to increase from 60 A to 65 A. At 70 A, the number of porosities decreased again. The maximum coating thickness was observed on samples prepared at 40 A, and the relationship between thickness and current was approximated by a third order polynomial function. The maximum depth of penetration of the melt pool was observed at 60 A and the relationship was approximated by a quadratic polynomial with an accurate closeness of fit of 0.9. The quadratic model showed that the depth of penetration generally increased with current to a maximum value and then dropped gradually with an increase in current.

Acknowledgements

The authors of this article wish to acknowledge the financial and technical support offered by Dedan Kimathi University of Technology and University of Johannesburg, South Africa, in actualization of this research work for publication.

Reference

[1] Gebert, A., & Bouaifi, B. (2006). Surface Protection by Means of Build-up Welding. Modern Surface Technology, 263-296
[2] Kumar, K., Deheri, S. C., & Masanta, M. (2019). Effect of Activated Flux on TIG Welding of 304 Austenitic Stainless Steel. Materials Today: Proceedings, 18, 4792-4798
[3] Chen, S., Huang, Y., Zhou, C., & Gu, P. (2019). Experimental and numerical study on fatigue performance of U-rib connections. Journal of Constructional Steel Research, 163, 105796.
[4] Zhang, C., Bao, Y., Zhu, H., Nie, X., Zhang, W., Zhang, S., & Zeng, X. (2019). A comparison between laser and TIG welding of selective laser melted AlSi10Mg. Optics & Laser Technology, 120, 105696.
[5] Park, J. H., Kim, Y. H., Baek, H. J., & Cho, S. M. (2019). A study on process development of super-TIG welding for 9% nickel steel with alloy 625. Journal of Manufacturing Processes, 40, 140-14
[6] Shrivas, S. P., Vaidya, S. K., Khandelwal, A. K., & Vishvakarma, A. K. (2020). Investigation of TIG welding parameters to improve strength. Materials Today: Proceedings.
[7] Moi, S. C., Rudrapati, R., Bandyopadhyay, A., & Pal, P. K. (2019). Design Optimization of Welding Parameters for Multi-response Optimization in TIG Welding Using RSM-Based Grey Relational Analysis. In Advances in Computational Methods in Manufacturing (pp. 193-203). Springer, Singapore.
[8] Chen, C., Fan, C., Cai, X., Lin, S., Liu, Z., Fan, Q., & Yang, C. (2019). Investigation of formation and microstructure of Ti-6Al-4V weld bead during pulse ultrasound assisted TIG welding. Journal of Manufacturing Processes, 46, 241-247.
[9] Garg, H., Sehgal, K., Lamba, R., & Kajal, G. (2019). A Systematic Review: Effect of TIG and A-TIG Welding on Austenitic Stainless Steel. In Advances in Industrial and Production Engineering (pp. 375-385). Springer, Singapore.
[10] Komshin, A. S., & Medvedeva, O. V. (2014). Measurement Control of the Degradation of the Properties of the Structural Materials of Shaft Lines. Measurement Techniques, 57(5), 526-532.
[11] Tanasković, D., Đorđević, B., Tatić, U., Sedmak, A., & Opačić, M. (2017). Repair Welding of Gear Shafts of Service Rollers at the Železara Smederevo. 8th International Scientific Conference IRMES: Machine Elements and Systems in Energy Sector Development of Power Production Systems, September, 365–370.
[12] Glibovitskii, B. E., Pikh, V. S., & Serivka, Y. V. (1984). Use of gas flame spraying of composite nickel-aluminum wire for repair of the worn points of shafts. Soviet materials science: a transl. of Fiziko-khimicheskaya mekhanika materialov/Academy of Sciences of the Ukrainian SSR, 20(3), 304-306.
[13] Sadeq, B. R., Sahib, B. S., & Alher, M. (2020). Study of the Effects of Welding Process on the Microstructure of Worn Carbon Steel Shaft. IOP Conference Series: Materials Science and Engineering, 671(1).
[14] Tanasković, D., Đorđević, B., Sedmak, S., & Mihajlo, A. (2018). The effect of exploitation conditions on the damage of a roller reducer toothed shaft and its repair. Machine Design, 10(4), 157–162.

[15] Tanasković, D., Dordevic, B., Gajin, M., Arandelović, M., & Gostović, N. (2018). Damages of burner pipes due to the working conditions and its repair welding. Procedia StructuralIntegrity,13(January2018),404–409.
[16] Milovanović, N., Dordević, B., Tatić, U., Sedmak, S., & Štrbački, S. (2017). Low-temperature corrosion damage and repair of boiler bottom panel tubes. Structural Integrity and Life, 17(2), 125–131.
[17] Mondal, A., Kumar Saha, M., Hazra, R., & Das, S. (2016). Influence of heat input on weld bead geometry using duplex stainless-steel wire electrode on low alloy steel specimens. Cogent Engineering, 3(1), 1143598.
[18] Rashid, R. R., Abaspour, S., Palanisamy, S., Matthews, N., & Dargusch, M. S. (2017). Metallurgical and geometrical characterisation of the 316L stainless steel clad deposited on a mild steel substrate. Surface and Coatings Technology, 327, 174-184.